The fluidized bed air heat exchanger in a hybrid Brayton-cycle solar power plant

Cite as: AIP Conference Proceedings **2126**, 140002 (2019); https://doi.org/10.1063/1.5117650
Published Online: 26 July 2019

Shuo Li, Weibin Kong, Huili Zhang, Florian Sabatier, Renaud Ansart, Gilles Flamant, and Jan Baeyens

The Fluidized Bed Air Heat Exchanger in a Hybrid Brayton-Cycle Solar Power Plant

Shuo Li[1, a)], Weibin Kong[1, b)], Huili Zhang[1, c)], Florian Sabatier[2, d)], Renaud Ansart[2, e)], Gilles Flamant[3, f)], Jan Baeyens [4, g)]

[1] *Beijing University of Chemical Technology, School of Life Science and Technology, 15# Beisanhuan east road, Beijing, China*
[2] *Laboratoire de Génie Chimique, Université de Toulouse, CNRS, Toulouse, France*
[3] *PROMES-CNRS, Route du Four Solaire 7, Odeillo-Font Romeu, France*
[4] *European Powder and Process Technology, Park Tremeland 9, Tremelo, Belgium*

[a)]ssurel@163.com
[b)]kongweibin2012@gmail.com
[c)]zhhl@mail.buct.edu.cn
[d)]florian.sabatier@ensiacet.fr
[e)]ransart@ensiacet.fr
[f)]Corresponding author: Gilles.Flamant@promes.cnrs.fr
[g)]Corresponding author: EuroPPT@gmail.com

Abstract. Using group A particle suspensions as heat transfer fluid in concentrated solar power plants leads to higher efficiency and lower costs. Combined cycle power generation becomes possible with e.g. a topping Brayton air turbine cycle and an advanced steam power block as bottoming cycle. This hybrid combined cycle solar tower power plant will be tested on a 3 MW_{th} pilot-scale at the CNRS-Themis solar tower (France) with the receiver, hot powder storage and air Brayton turbine. The suspension will exit the receiver at a nominal outlet temperature of 750-800°C. Hot powders will be stored and will subsequently exchange heat with the turbine air. The outlet temperature of the air heat exchanger (625 to 700 °C) will considerably determine the hybrid operation (reducing the possibly used fossil fuel boost) and the heat exchanger design is of paramount importance. The air heat exchanger will be a baffled cross-flow fluidized bed. Air will be heated in an in-bed finned-tube bundle. Air will be fed at 5.8 bar and ~ 270°C. The hydrodynamics and heat transfer characteristics of the air heat exchanger were experimentally investigated towards bubble properties and heat trasnfer coefficient. The bed to tube heat transfer coefficient was measured for different pipe geometries at bed temperatures up to 700 °C, exceeding 2 kW/m^{2}K for a twin-bore finned tube but only about 650 W/m²K for the bare tube of equal outside diameter. The heat transfer coefficient from the tube wall to the turbulent air flow inside the tube (~ 325 W/m^{2}K) determines the design. NEPTUNE_CFD software was used to perform 3D- numerical simulations of the fluidized bed hydrodynamics via an Eulerian n-fluid approach. Simulation and experimental results were in very fair agreement, stressing the capability of mathematical models to predict the behaviour of a cross-flow bubbling fluidized bed.

INTRODUCTION

Concentrated Solar Power (CSP) uses heliostats to focus solar irradiation onto a receiver where a heat transfer fluid (HTF) is used as heat collector and carrier [1–3]. Although currently more expensive than other renewable energy sources such as photovoltaic cells and wind turbines, improvements can reduce operating costs and make CSPs more competitive by exploiting their advantages of possible hybridization, high efficiency, ease of thermal energy storage, and good scale-up potential [1–5]. The key to further economies is to operate at higher temperatures, allowing higher power conversion efficiencies and higher storage temperatures with increased energy storage density [3]. This fostered the development of using particle suspensions as HTF [1–5]. The increased thermodynamic efficiency will moreover

SolarPACES 2018
AIP Conf. Proc. 2126, 140002-1–140002-8; https://doi.org/10.1063/1.5117650
Published by AIP Publishing. 978-0-7354-1866-0/$30.00

reduce the heliostat field and energy storage, recognized as more efficient and less expensive. Higher HTF temperatures offer possibilities for using advanced power generation concepts, such as the air or supercritical CO_2 Brayton cycles, in combination with an advanced steam Rankine cycle in a complete combined cycle generation concept. Group A powders (mostly between 30 and 75 μm) are applied in fluidized bed solar receivers [1,5] since operating at low superficial gas velocities (low sensible heat loss) and producing a considerable particle mixing [1]. They are moreover easily circulated around moving bed, fluidized bed and pneumatic conveying loops. Fig. 1 depicts the layout of the investigated hybrid combined cycle solar tower power plant. The top cycle (Air Brayton) will be tested at pilot-scale in the CNRS-Themis solar tower (France) [6]. The heliostat field concentrates solar radiation atop the tower, where a set of vertical tubes form a particle suspension loop receiver. The particle suspension is fluidized with air (Al) and conveyed upward. It is then collected in the hot particle storage and fed to a crossflow fluidized bed air heat exchanger. The air-turbine cycle includes several parts. Ambient air (GT1) enters the turbine compressor (TC) and is compressed to pressure and temperature conditions of GT2. After being pre-heated to the temperature GT3, fossil fuel (F1) is possibly added in a separate combustor to boost the air-temperature to GT4 in order to increase the turbine efficiency.

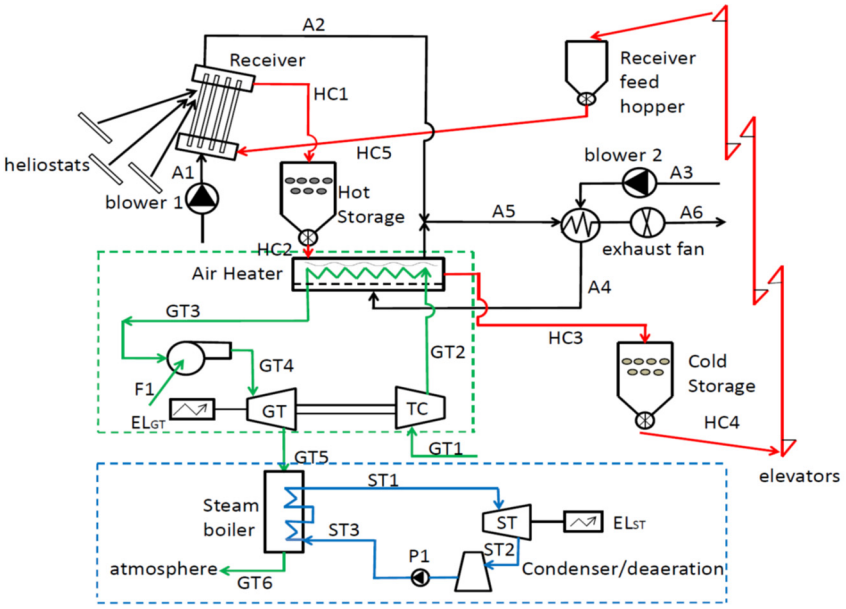

FIGURE 1. Schematics of a solar tower combined cycle generation process [7]

The powder receiver will have a nominal outlet temperature of 750 to 800°C. The outlet temperature of the air heat exchanger will determine the hybrid operation (reducing the possibly used fossil fuel boost) and the design of this heat exchanger is of paramount importance.

DESCRIPTION OF THE AIR PREHEATER AND RESEARCH OBJECTIVES

The air heat exchanger will be executed as a baffled cross-flow fluidized bed (Fig. 2, using an in-bed externally finned-tube bundle. Air will be fed from the turbine compressor at 5.8 bar. With reference to Fig. 1, the heat balance for air and particles over the air pre-heater is fixed

$$F_a C_{pa}(T_{GT3} - T_{GT2}) = F_{HC2} C_{pa}(T_{HC2} - T_{HC3}) \quad (1)$$

T_{GT2} is determined by the turbine compressor characteristics, but will be around 270-280 °C. The particle feed temperature will be varied from 750 to 800°C. The air outlet temperature will then vary from 625 to 700°C. Once flow rates and temperatures have been determined, the required temperature boost of the turbine inlet to T_{GT4} by fossil fuel combustion is fixed. The pressure drop for the air flow in the tubes follows the Darcy-Weisbach equation, with values of the friction factor according to the Blasius equation. Two sets of experiments were carried out in

order to experimentally investigate the hydrodynamics and heat transfer characteristics of the air heat exchanger. Additionally, NEPTUNE_CFD software was used to perform 3D- numerical simulations of the fluidized bed hydrodynamics via an Eulerian n-fluid approach.

EXPERIMENTAL INVESTIGATION

Hydrodynamics

Due to the difficulty and expense involved in measuring bubble sizes directly in 3D beds with X-rays or other means, a 2D bed was built to represent what would be observed by cutting a vertical slice through a bed of square cross-section. Such an assumption seems reasonable and has been made when predicting conversions in fluidized bed chemical reactors. Given suitable lighting, bubbles can readily be seen and imaged by high speed camera (Panasonic HDC-TM40). The 2D bed was 50cm × 2cm in cross-section and constructed of Perspex. A calibrated digital flow meter (MF5712-N-200, Siargo) was used to measure air flow rates. Pressure drops were measured using water manometers. The 2D bed was operated without and with tubular array being present, as illustrated in Fig. 3. Different tube-geometries were examined. The bed height was max 0.4m and high-speed imaging was conducted at different positions along the width and height in the column. The powder used was crystobalite having a narrow size range with d_{sv} of 85 μm and density of 2740 kg/m^3. The minimum fluidization velocity U_{mf} was found to be 1.1 cm/s, ~25% higher than in a 3D-bed due to the 2D wall effects, but independent of bed depth. The video images were analyzed for bubble properties. The sizes of at least 30 bubbles were measured at each flow rate and at different bed depths. The mean size was determined. Bubble frequencies were also taken from the imaging. Three equally spaced points in a horizontal plane (at approximately 13cm intervals) and at 5 successive levels in the bed were sampled. A bubble that enclosed a monitoring point was counted.

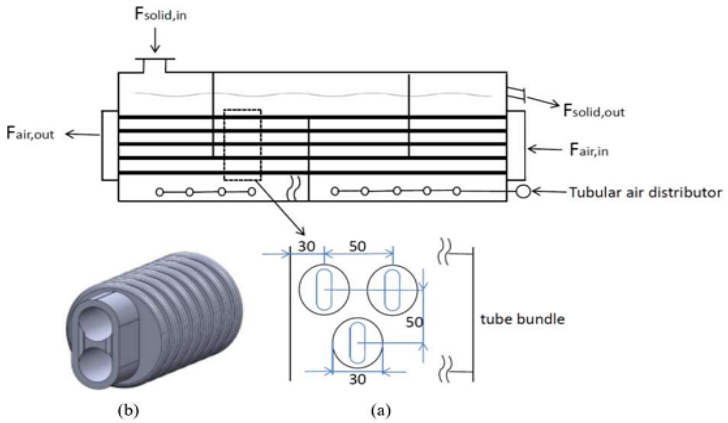

FIGURE 2. Air heat exchanger design (a), with illustration of the twin-bore finned air pipe (b)

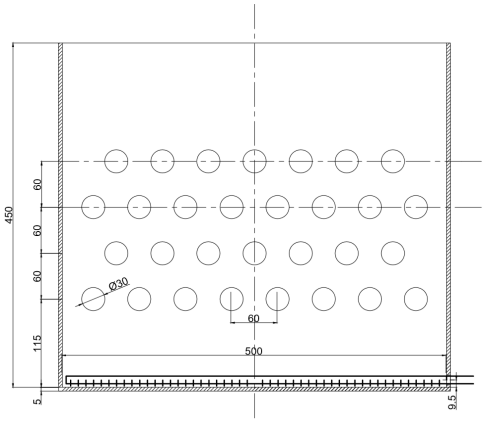

FIGURE 3. Experimental 2D-rig

Heat Transfer Measurement

The experiments applied a well-insulated rectangular FB with cross-sectional area of 9cm × 23cm, with a tubular distributor of two perforated pipes having 1 cm outside diameter and 1 mm of perforated orifices. As heat exchange element, various heat transfer tube geometries were tested and placed in the middle of the bed. As bed material, the same crystobalite is employed, and the bed height is kept around 25 cm. The sand is heated to 700℃ in a furnace and poured into the bed. To measure a high heat removal, water was used instead of air. A constant water flow was maintained inside the tube to monitor the absorbed heat. Thermocouples were placed inside the bed, on the outer tube wall, and in the feed and discharge of the water. Temperatures were recorded periodically. The water flow rate (m) was maintained at a constant value. The heat absorbed is given by:

$$Q = mCp_w \Delta T_w \tag{2}$$

where ΔT_w is the temperature difference between inlet and outlet of water.

This heat is also equal to the heat transferred from the fluidized bed to the water through the finned tube, and is given by:

$$Q = UA\Delta T \tag{3}$$

ΔT being the temperature difference between the tube wall (exposed surface area A) and the mean temperature of the water inside the tube. U is the overall heat transfer coefficient. The measurements were taken for bed temperatures between 650 °C and 150 °C.

Neptune_ Code Description

Three-dimensional numerical simulations used the code NEPTUNE_CFD. This Eulerian n-fluid unstructured parallelized multiphase flow software has been developed in the framework of the NEPTUNE project financially supported by the "Commissariat à l'Energie Atomique", by "Electricité de France", by the "Institut de Radioprotection et de Sureté Nucléaire", and by AREVA-NP [8]. The modelling approach for poly-dispersed fluid particle flows is implemented by the "Institut de Mécanique des Fluides de Toulouse". The numerical solver was developed for High Performance Computing [9]. The Eulerian n-fluid approach used is a hybrid method [10] in which the transport equations are derived by grouped averaging conditioned by the phase presence for the continuous gaseous phase and by use of the kinetic theory of granular flows supplemented by fluid effects for the dispersed phase. The momentum transfer between gas and particle phases is modelled using the drag law of Wen and Yu [11], limited by the Ergun equation[12] for dense flows [12–14]. The collisional particle stress tensor is derived in the frame of the kinetic theory of granular media [15]. In this study the gas flow equations are treated considering a laminar regime because the gas Reynolds stress tensor in the momentum equation is negligible compared to the drag term. For the solid phase, a transport equation for the particle random kinetic energy, q_p^2, is solved. The quasi-static granular flow zones are taken into account in the particle stress tensor by the additional frictional stress tensor [16]. All the equations for the hydrodynamics are detailed by Ansart et al. [17]. The numerical simulations consider the impact of the finned-tube bundle on the gas-particle flow hydrodynamics without coupling with heat transfer. Three meshes composed of hexahedra were realized. The 2D bed was meshed without and with tubular array being present. Two different cases were examined with the tube bundle: with round tubes and twin-bore tubes. The dimensions are exactly the same as the experimental mockups. Particular attention has been paid to the cells around the tubes in order to capture the structures at meso-scale.

RESULTS AND DISCUSSION

Bed Hydrodynamics

Without tubes being present, the imaging enabled to determine bubble diameter and bubble frequencies at different locations in the 2D-bed. Results are illustrated in Fig. 4. Equations were developed and resulted in: $d_B = d_{BO} + 0.057H^{0.34}$, with d_{B0}, the initial bubble size formed at the distributor with N_{or} number of holes per m^2 of bed cross sectional area, and calculated as [18]:

$$d_{BO} = \frac{1.3[\frac{U - U_{mf}}{N_{or}}]^{0.4}}{g^{0.2}} \quad (4)$$

The bubble frequency was found to be fitted by the 2-phase theory [18]:

$$f = 1.5\frac{U - U_{mf}}{d_B} \quad (5)$$

Although measured in a 2D-bed, bubble sizes and frequencies do not considerably differ from 3D equivalent measurements, since bubble growth in deeper beds of group A powders is limited by a combined action of coalescence and splitting.

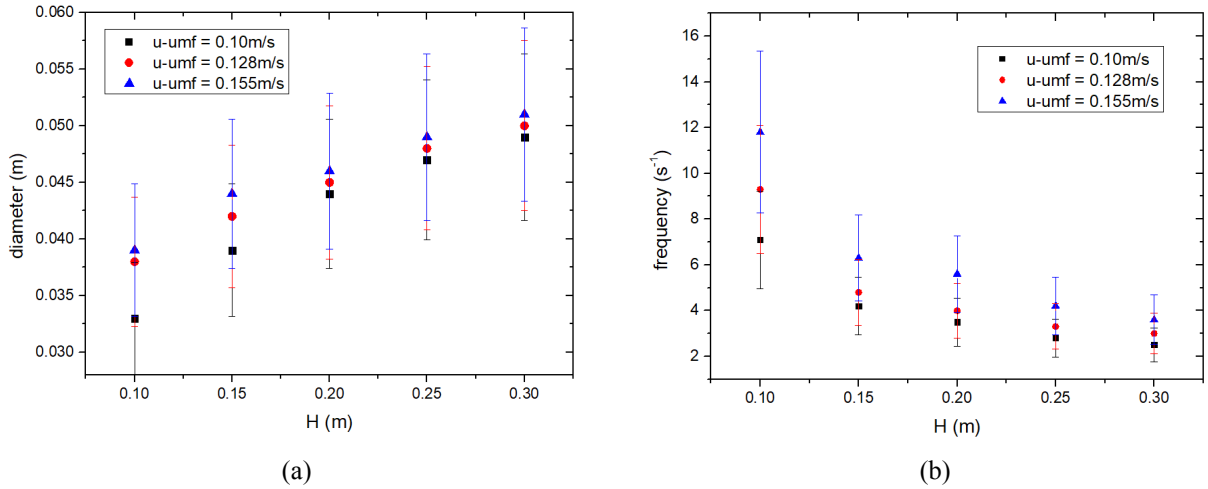

FIGURE 4. Bubble sizes (a) and frequencies (b) versus bed height at given excess velocities

With tubes present, the bubble sizes appear to be limited by the effective pitch between the tubes, and only frequencies increased with air velocity. The bed level above 0.15 m, hence within the tube bundle, had little effect. With traditional round tubes, particles hardly moved on the top of the tubes, creating a significant dead-zone as the red triangle shows in fig. 5(a). An air gap was clearly seen at the lower tube part. The novel twin-bore tube (see also Fig. 6 with open fin arrangement allowed bubbles to move to the tube-core, with frequent re-coalescence and a very limited dead-zone. Whereas bubble sizes in the twin-bore tube were about 4.0±0.2cm, they were 3.4±0.2cm with the round tubes.

(a) (b)

FIGURE 5. Bubbles with round tube (a) and twin-bore tube (b) versus bed height

Heat Transfer

The heat transfer coefficient from bed-to-wall was measured for the 3 tube geometries, and results are shown in Fig. 6. The fluid velocity inside the tubes was kept constant for all geometries. The heat transfer from the tube wall to the turbulent fluid flow was separately determined, and was in excellent agreement with predictions by the Gnielinski equation. Finned tubes considerably increase the heat transfer coefficient through the larger surface area exposed to the bed. The twin-bore pipe results confirm the influence of the hydrodynamics and the absence of a stagnant particle nose and gas film enhanced the heat transfer in comparison with the round tubes. Since the heat exchanger will be of externally finned tube design with a high bed-to-wall heat transfer coefficient (>> 2 kW/m^{2}K) [12], the overall heat transfer is determined by the wall-to-in-tube air flow. At air velocities of 35 to 40 m/s at the exit T of ~ 650-750 ℃, Gnielinski predicts air-side transfer coefficients of ~ 325 W/m^{2}K.

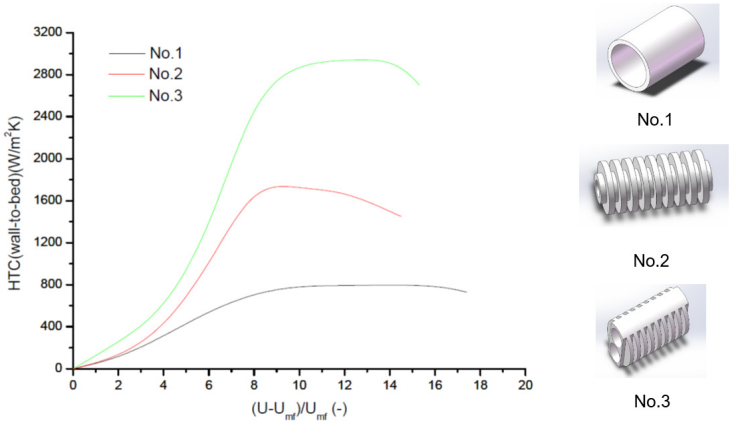

FIGURE 6. Fluidized bed-to-wall heat transfer coefficient for different tube geometries

Neptune CDD Simulations

The initial simulation results for the round and twin-bore tube are illustrated below. They confirm that round tubes are more prone to form a static solid layer on the top, and a gas film at the bottom of the tube. With the twin-bore tubes, the extent of these heat-transfer limiting phenomena decreases.

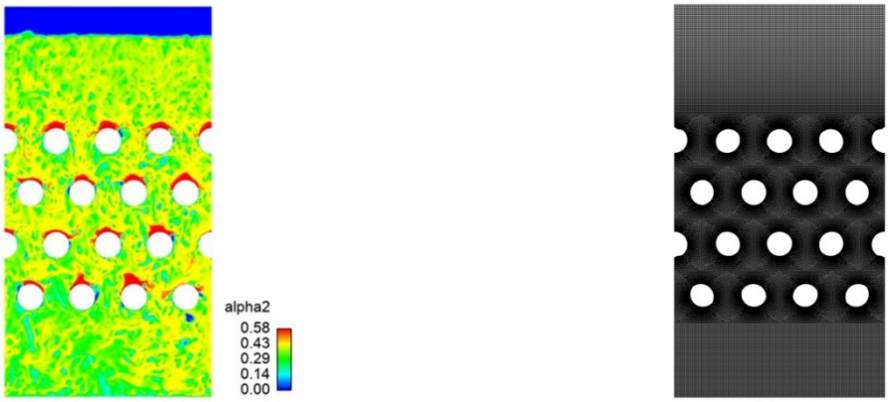

(a) (b)

FIGURE 7. Simulation for fluidized bed with round heat-transfer tubes

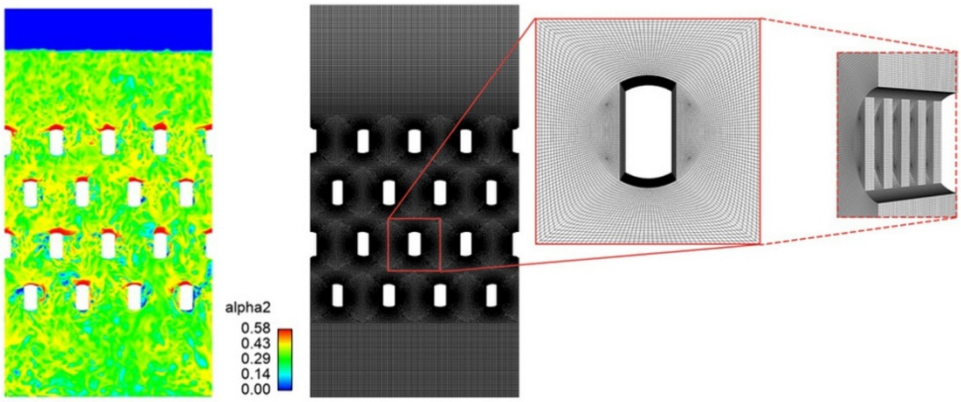

FIGURE 8. Simulation for fluidized bed with twin-bore heat-transfer tubes

CONCLUSIONS

The use of a crossflow bubbling fluidized bed with in-bed tubular array was experimentally investigated towards hydrodynamics (bubbling) and heat transfer. Bubble sizes and frequencies were measured from high speed imaging and correlated, with and without tubular array being present. The geometry of the tube bundle is important. The heat transfer coefficient from the bed to the finned tube wall exceeds 2kW/m^{2}K. The heat transfer coefficient from the tube wall to the turbulent air flow (~325 W/m^{2}K) hence determines the heat exchanger design. NEPTUNE_CFD software simulation and experimental results were in very fair agreement, stressing the capability of mathematical models to predict the behaviour of a cross-flow bubbling fluidized bed.

ACKNOWLEDGEMENTS

This work was supported by the Beijing Advanced Innovation Center for Soft Matter Science and Engineering of the Beijing University of Chemical Technology and funding was obtained from the European Union's Horizon 2020 research and innovation program under grant agreement 727762, project Next-CSP.

REFERENCES

1. H.L. Zhang, H. Benoit, D. Gauthier, J. Degrève, J. Baeyens, I.P. López, M. Hemati, and G. Flamant, Appl. Energy **161**, 206 (2016).
2. *International Energy Agency. Technological Roadmap Solar Thermal Electricity* (IEA-publication, 2014).
3. H.L. Zhang, J. Baeyens, G. Cáceres, J. Degrève, and Y. Lv, Prog. Energy Combust. Sci. **53**, 1 (2016).
4. H. Zhang, H. Benoit, I. Perez-Lopez, G. Flamant, T. Tan, and J. Baeyens, Renew. Energy **111**, 438 (2017).
5. G. Flamant, D. Gauthier, H. Benoit, J.-L. Sans, R. Garcia, B. Boissière, R. Ansart, and M. Hemati, Chem. Eng. Sci. **102**, 567 (2013).
6. New EU Horizon 2020 Research Programme (Next CSP), (2017).
7. Q. Kang, R. Dewil, J. Degrève, J. Baeyens, and H. Zhang, Energy Convers. Manag. **163**, 292 (2018).
8. N. Méchitoua, M. Boucker, J. Laviéville, S. Pigny, and G. Serre, in *NURETH 10* (Seoul, South Korea, 2003).
9. L. Bennani, H. Neau, J. Baudry, J. Laviéville, P. Fede, and O. Simonin, Chem. Eng. Res. Des. **120**, 333 (2017).
10. S. Morioka and T. Nakajima, J. Theor. Appl. Mech. **6**, 77 (1987).
11. C. Wen and Y. Yu, Chem. Eng. Symp. Ser. **62**, 100 (1965).
12. S. Ergun, Chem. Eng. Prog. **48**, 89 (1952).
13. A. Gobin, H. Neau, O. Simonin, J.-R. Llinas, V. Reiling, and J.-L. Sélo, Int. J. Numer. Meth. Fluids **43**, 1199 (2003).
14. F. Audard, O. Simonin, P. Fede, and F. Belut, in *ASME/JSME/KSME 2015 Jt. Fluids Eng. Conf. AJKFFluids* (2015).
15. A. Boelle, G. Balzer, and O. Simonin, in *ASME, Fluids Eng. Div. FED* (1995), pp. 9–18.
16. A. Srivastava and S. Sundaresan, Powder Technol. **129**, 72 (2003).
17. R. Ansart, P. García-Triñanes, B. Boissière, H. Benoit, J.P.K. Seville, and O. Simonin, Powder Technol. **307**, 25 (2017).
18. W.B. Kong, T.W. Tan, J. Baeyens, G. Flamant, and H.L. Zhang, Ind. Eng. Chem. Res. **56**, 4136 (2017).